25th ABCM International Congress of Mechanical Engineering
October 20-25, 2019, Uberlândia, MG, Brazil

COB-2019-1563
INNOVATIVE FOOT PRESSURE SENSOR DESIGN FOR HUMANOID ROBOTS

Francisco Arthur Bonfim Azevedo
Daniela Vacarini de Faria
Marcos R. O. A. Maximo
Maurício Vicente Donadon
Instituto Tecnológico de Aeronáutica, Praça Mal. Eduardo Gomes, 50, Vila das Acácias, CEP: 12228-900, São José dos Campos - SP - Brazil
arthurazevedo41@gmail.com, danivacarini@gmail.com, mmaximo@ita.br, donadon@ita.br

Abstract. *In this paper, a novel foot sensor for measuring the center of pressure (CoP) for humanoid robots is presented. The foot sensor consists of a monolith design, with four bending beam load cells. The bending strain is measured through four pairs of strain gauges in half bridge configuration. The final geometry was achieved through topological optimization. Experimental results show good correlation with predicted and measured CoP position.*

Keywords: *humanoid robots, sensors, legged locomotion, topological optimization, center of pressure.*

1. INTRODUCTION

In recent decades, mobile robotics has faced an increasingly development in legged locomotion. Along with the groundbreaking works from Raibert *et al.* (1983) and from Honda (Hirai *et al.*, 1998) in its E-series robots, one can also cite more recent models that have been developed such as Honda ASIMO (Sakagami *et al.*, 2002), Boston Dynamics Atlas (Atmeh *et al.*, 2014), and NASA Valkyrie (Radford, 2015).

Some interesting work has been developed for robot competitions, which demand quick and precise locomotion for target following. One such competition is the RoboCup, for which the ITAndroids team from the Aeronautics Institute of Technology (ITA), Brazil, has developed a series of humanoid robots for the RoboCup Humanoid KidSize League. The robot *Chape* was designed by ITAndroids and is based on the open source Robotis OP2 project (Ha *et al.*, 2013).

In order to achieve a stable locomotion, one important concept is the *zero moment point* (ZMP). The ZMP is the point on the ground in which the ground reaction force does not produce any horizontal moment. A known stability rule in legged locomotion states that a robot is always stable if the ZMP does not leave the support polygon (the convex hull of the contact points between the feet and the ground) (Vukobratović and Okhocimskii, 1975). Although the ZMP location can be estimated by fusing data from the inertial measurement unit and the joint encoders, this estimate often suffers from the inherent difficulty of accurately modeling the many physical parameters present in a humanoid robot (Rotella, 2018).

To overcome this problem, many authors have developed sensors capable of measuring the center of pressure (CoP) of the foot. While the robot is not falling down, the ZMP and CoP coincide, thus one may use the CoP as a substitute for the ZMP. Among many different designs found on the Literature, the sensors may be categorized in: (a) 6-axis force and torque transducers (Schickl *et al.*, 2016), usually located at the ankle joint, (b) planar pressure sensors (S. Kagami, 2004), usually consisting on a matrix of force sensitive resistors (FSR) or piezoelectric sensors, and (c) planar strain sensors (Gregoire Passault, 2015).

In this paper, we contribute by presenting a new ZMP planar strain sensor design. This type was preferred over the 6-axis transducer type due to its lower price and ease of manufacture. The planar pressure sensor type was also avoided, since the Chape robot frequently walks over synthetic grass, thus it has studs similar to those found on soccer cleats. The innovative design consists of a single aluminum plate, shaped in a X-like configuration. Each part of the X is a bending beam load cell that links a stud to the ankle joint, and is equipped with two strain gauges in a half bridge configuration. The bending beams positions were obtained through topological optimization.

2. SENSOR DESIGN

This section presents the sensor design.

2.1 System Requirements

Since the robot should comply with the RoboCup Humanoid KidSize rules (Comitee, 2018), the feet are subject to some geometric constraints. According to the rules, each foot must fit into a rectangle of area A_{max}, according to Eq. (1):

$$A_{max} = \frac{1}{32}\left(2.22 H_{CoM}\right)^2, \tag{1}$$

where H_{CoM} denotes the height of the robot's center of mass in centimeters, measured in the upright posture. Since the height of the center of mass of the robot (CoM) is 28 cm, a maximum area of 118.58 cm^2 is allowed.

To obtain the normal loads suffered by the feet, we performed a simulation on the robotics simulator Gazebo. The simulation consists on a virtual model of the Chape robot, with the same walking control algorithm as the real one. The maximum force on each foot is 70N. A safety factor of 45% was used. Also, the sensor must be capable of measuring forces from 0 to 30 N in each stud, and this range must lie in the linear elastic region of the material.

Moreover, the team is aiming at a design that has low coupling among the measurements of each sensor and is easy to manufacture and assembly. Also, in order to be able to walk on the grass, studs of at least 20 mm of height should be used.

2.2 Geometry Design and Parametric Optimization

A series of different geometries of feet was designed with beams that connect the ankle to the studs. Figure 1 shows some of the tested designs. Therefore, structural simulations were performed, using the software SolidWorks, and a long process of parametric optimization of holes, thickness of the metal, and other parameters, seeking the optimal point between simplicity, lightness and robustness, was executed.

Finite Element Method (FEM) simulations were executed on the four beams. They considered the impact of the robot's foot on the ground while walking and the weight of the robot standing in one of the studs, which was considered the worst case. The results of the simulation of all four designs may be seen in Fig. 1.

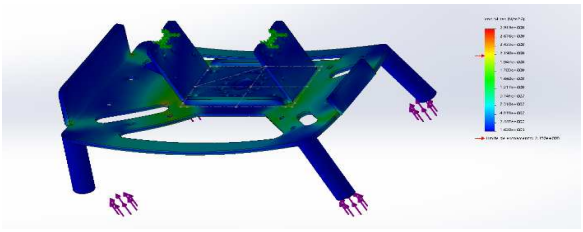

(a) First part.

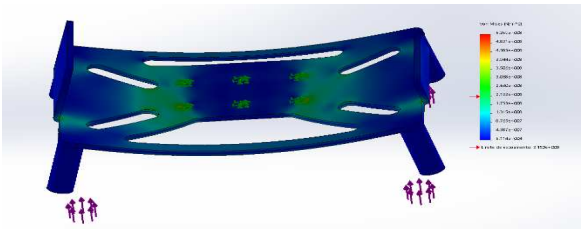

(b) Second part.

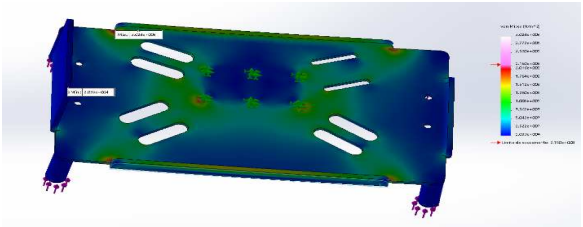

(c) Third part.

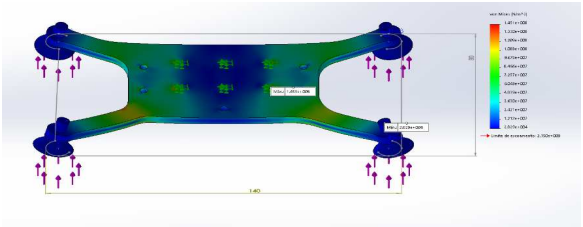

(d) Fourth part.

Figure 1: Results of the structural simulation on each one of the parts.

Although the versions (a), (b) and (c) had overall higher rigidity compared to the version (d), using the same sheet thickness, they tended to present higher coupling among the forces measured on each stud. The lower rigidity was addressed by increasing the metal sheet thickness compared to the other versions. Also, the more simple design of version (d) was easier to manufacture and the four beams allowed easier placement of the strain gauges on the foot. These properties are important since the laboratory has four similar robots and it is important that they have similar behaviors. The authors assume that this will make the sensors easier to calibrate and more predictable to be used on a closed loop control of the robot's walking algorithm.

The selected geometry was subsequently used to make the mathematical modeling of the project.

2.3 Mathematical Modeling

For the mathematical model, the coordinate system was placed on the center of the ankle joint, as may be seen in Figure 2.

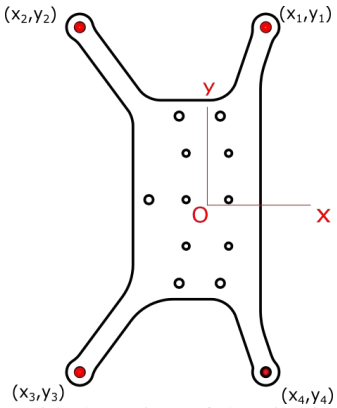

Figure 2: Coordinate system set on the foot, with the points of the pins indicated by $(x_1,\ y_1)$, $(x_2,\ y_2)$, $(x_3,\ y_3)$, and $(x_4,\ y_4)$.

The resulting force F_r as a function of the reaction forces in each pin, F_1, F_2, F_3, and F_4, is obtained by Eq. (2) and the resulting momentum on the center of the coordinate system $\overrightarrow{M}_{iO}$ may be seen in Eq. (3).

$$\overrightarrow{F}_r = \overrightarrow{F}_1 + \overrightarrow{F}_2 + \overrightarrow{F}_3 + \overrightarrow{F}_4, \tag{2}$$

$$\overrightarrow{M}_{iO} = \overrightarrow{r}_i \times \overrightarrow{F}_i = (x_i\hat{i} + y_i\hat{j}) \times (\left\|\overrightarrow{F}_i\right\| \hat{k}) = \left\|\overrightarrow{F}_i\right\| (y_i\hat{i} + x_i\hat{j}). \tag{3}$$

By the definition of center of pressure, considered as the point (x_c, y_c), the sum of the resulting moments, M_c in that point must be zero. Thus, it was obtained the matrix Equation (4).

$$[M_c] = \left(\begin{bmatrix} x_1 & x_2 & x_3 & x_4 \\ y_1 & y_2 & y_3 & y_4 \end{bmatrix} - \begin{bmatrix} x_c & x_c & x_c & x_c \\ y_c & y_c & y_c & y_c \end{bmatrix} \right) \begin{bmatrix} F_1 \\ F_2 \\ F_3 \\ F_4 \end{bmatrix}, \tag{4}$$

or in the condensed form as shown in the Equation (5).

$$[M_c] = \left([X_i] - [X_c] \right) [F], \tag{5}$$

$$[X_i] = \begin{bmatrix} x_1 & x_2 & x_3 & x_4 \\ y_1 & y_2 & y_3 & y_4 \end{bmatrix}, \quad [X_c] = \begin{bmatrix} x_c & x_c & x_c & x_c \\ y_c & y_c & y_c & y_c \end{bmatrix}, \quad [F] = \begin{bmatrix} F_1 \\ F_2 \\ F_3 \\ F_4 \end{bmatrix}. \tag{6}$$

Applying the definition of center of pressure in the Equation (7):

$$[M_c] = \begin{bmatrix} 0 \\ 0 \end{bmatrix}. \tag{7}$$

Thus, solving the Equation (5), the Equation (8) is obtained.

$$\begin{cases} F_1(x_1 - x_c) + F_2(x_2 - x_c) + F_3(x_3 - x_c) + F_3(x_3 - x_c) = 0 \\ F_1(y_1 - y_c) + F_2(y_2 - y_c) + F_3(y_3 - y_c) + F_3(y_3 - y_c) = 0 \end{cases}. \tag{8}$$

From equation (8), we may obtain the position of the CoP $(x_c,\ y_c)$, as shown in Equation (9).

$$\begin{bmatrix} x_c \\ y_c \end{bmatrix} = \frac{1}{F_1 + F_2 + F_3 + F_4} \begin{bmatrix} x_1 & x_2 & x_3 & x_4 \\ y_1 & y_2 & y_3 & y_4 \end{bmatrix} \begin{bmatrix} F_1 \\ F_2 \\ F_3 \\ F_4 \end{bmatrix}. \tag{9}$$

Afterwards, the pair stud-beam and the strain-gauge were modeled as a Euler-Bernoulli beam (Beer and E. R. Johnston, 1982). Figure 3 shows a schematic representation of the system.

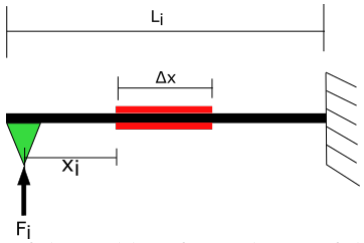

Figure 3: Diagram showing the conditions of the problem for each one of the bars. Strain gauges are shown in red, the pin is in green, and the bar in black.

Using the uni-dimensional approximation of Euler-Bernoulli theory, the strain in the beam can obtained as shown in Equation (10), where M is the bending moment, y is the distance from the neutral line, I is the moment of area and E is the material's young modulus.

$$\varepsilon = \frac{My}{IE}. \tag{10}$$

Applying in Eq. (10) the boundaries of Fig. 3, we obtain Eq. (11), where ε_i is the deformation in the beam "i".

$$\varepsilon_i = \frac{F_i h}{2I_i E}\left(x_i + \frac{\Delta x}{2}\right). \tag{11}$$

Thus, we have the Equation (12).

$$F_i = \frac{2I_i E}{h\left(x_i + \frac{\Delta x}{2}\right)}\varepsilon_i. \tag{12}$$

Moreover, using the concepts of the strain gauge sensor in Dally and Riley (1978), the deformation in the strain gauges may be obtained from the voltage signal ΔE as shown in the Equation (13), where GF is the strain gauge's Gauge Factor and V the input voltage of the sensor.

$$\varepsilon = \frac{2\Delta E}{GF \cdot V}. \tag{13}$$

Applying Eq. (13) in Eq. (12), we obtain Eq. (14).

$$F_i = \frac{4\Delta E_i}{GF \cdot V}\frac{2I_i E}{h\left(x_i + \frac{\Delta x}{2}\right)}. \tag{14}$$

Applying the definition of moment of area for rectangular section beams, we obtain $I = b_i h^3/12$. Thus, the force in each pin may be expressed by Eq. (15), where ΔE_i is the voltage reading in the sensor of the beam "i", b_i is the length of the bar i, h is the thickness of the beam, E is the young modulus of the material, GF is the gauge factor of the sensor, V is the input voltage of the sensor, x_i is the distance of the sensor to the pin, and Δx is the length of the sensor.

$$F_i = \frac{\Delta E_i}{3GF \cdot V}\frac{2b_i h^2 E}{\left(x_i + \frac{\Delta x}{2}\right)}. \tag{15}$$

3. EXPERIMENTAL RESULTS

Experimental tests were made in order to validate the design. At first, the foot was manufactured in AL 5052-H34 and the sensors were installed on it, as shown in Fig. 4.a. The foot was fixed in a platform and the loads in each stud were emulated by weights ranging from 100g to 3kg, Fig. 4.b shows this setup. The strain gauge's outputs were measured by a HBM acquisition system. The results are shown in Fig. 5.

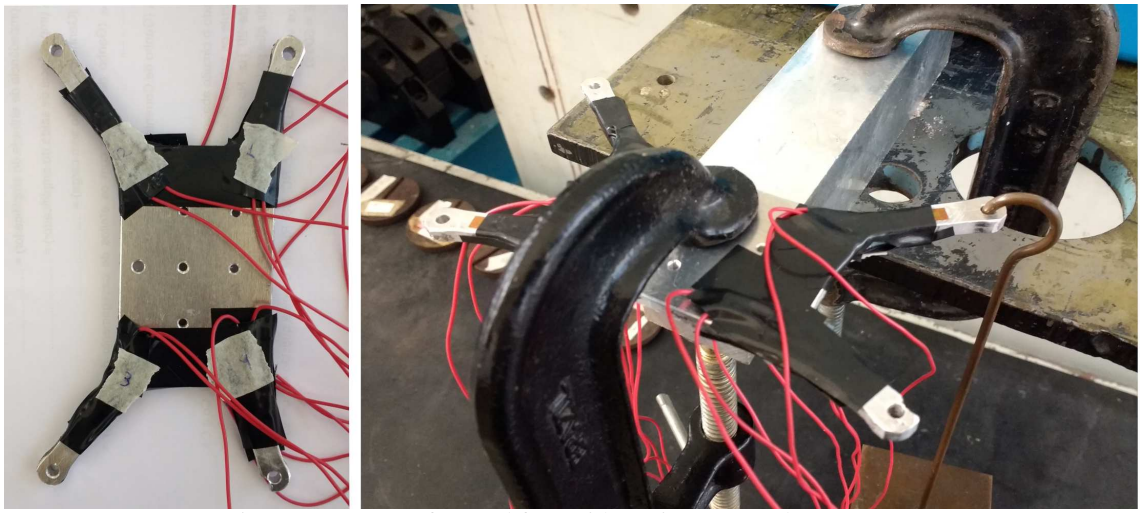

Figure 4: (a) manufactured foot with strain gauges; (b) test setup.

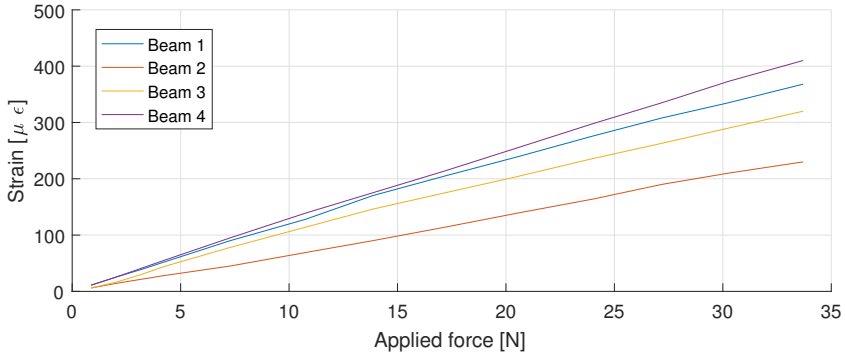

Figure 5: Experimental results

The experimental results show that the measured strains lie in the nearly linear region, as designed. Also, beams 1 and 4 have similar behaviour, as expected. The unwanted difference between beams 2 and 3 was caused by bad strain gauge placement. This problem is not critical to the project, but could lead to the need of exhausting sensor calibrations for each foot. To avoid this, markings for strain gauges will be added to the design.

Also, the force calculated by Eq. (12) was compared with the weight applied in the foot. The Figure 6 graphically the percentage comparison of the two forces.

Finally, by using the measures of the strain gauges and the equations (9) and (12), the position of the CoP in every of the 14 measures was estimated, obtaining the Figure 7.

Also, since the Gazebo simulation mentioned in Section 2. lis only able to consider the robot as infinitely rigid, it was difficult to estimate precisely if the deflections on the foot beams would impair the robot gait, unfortunately this effect could only be qualitative tested.

On the other hand, the feet structures were integrated with our humanoid robots and thoroughly tested in the laboratory and also in two humanoid robot soccer competitions, namely Latin American Robotics Competition 2018 and RoboCup 2019. Figure 8.a shows the robot whith the designed feet, Figure 8.b shows the robots during a soccer match in 2019 RoboCup, which took place in Sydney. This also helped showing that the foot design had a good robustness, being able to participate in these competitions without any occurrences.

4. CONCLUSION

This paper presented a novel foot structure for implementing a center of pressure sensor. After considering the requirements, different geometries were evaluated using FEM simulations and the best geometry based on simplicity, lightness, and robustness was selected. Moreover, experimental results show that the foot design is able to correctly predict the center of pressure after adequate strain gauge calibration.

Regarding future work, we are designing a printed circuit board (PCB) to integrate this foot sensor with our robot's data bus. Moreover, we are developing new state estimation and control algorithms which are able to take the center of pressure information into account.

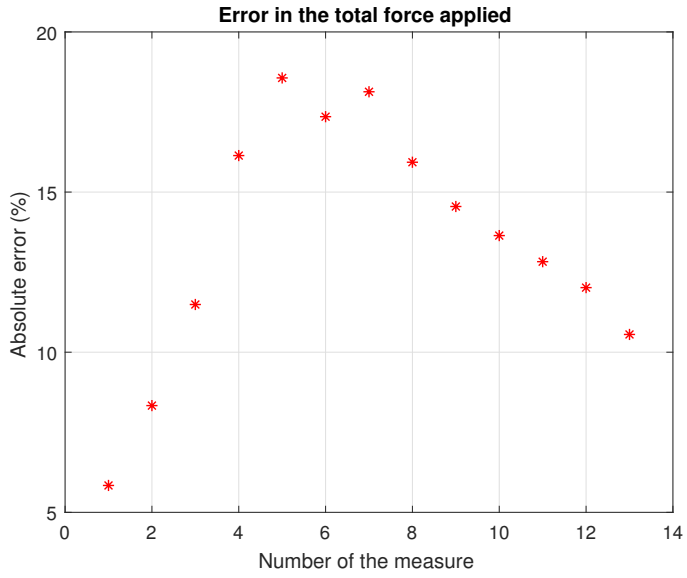

Figure 6: Percentage comparison between the force calculated and the weight applied in the foot.

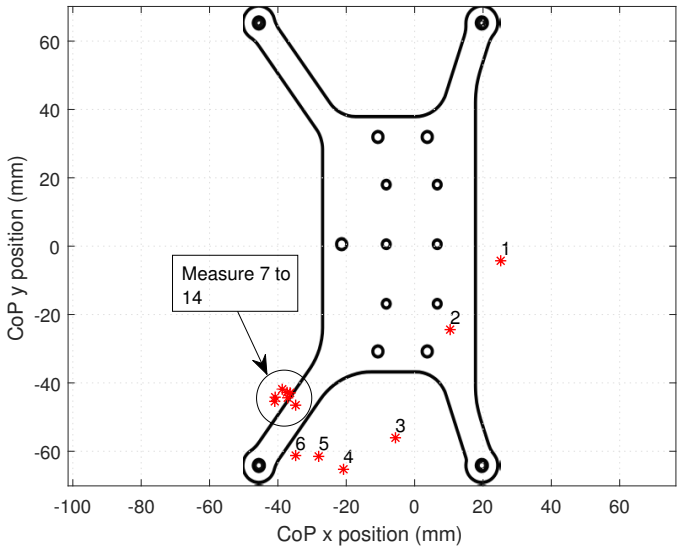

Figure 7: Position of the CoP in every of the 14 measures of the experiment.

5. ACKNOWLEDGEMENTS

Francisco Azevedo acknowledges the National Council for Scientific and Technological Development (CNPq) for his undergraduate research scholarship. Moreover, the team ITAndroids would like to thank its sponsors: Altium, Intel, ITAEx, Mathworks, Metinjo, Micropress, Polimold, Rapid, Solidworks, ST Microelectronics, TFG, and Virtual Pyxis. Finally, the authors are grateful to the Centro de Competência em Manufatura (CCM) for their support on manufacturing the foot prototype.

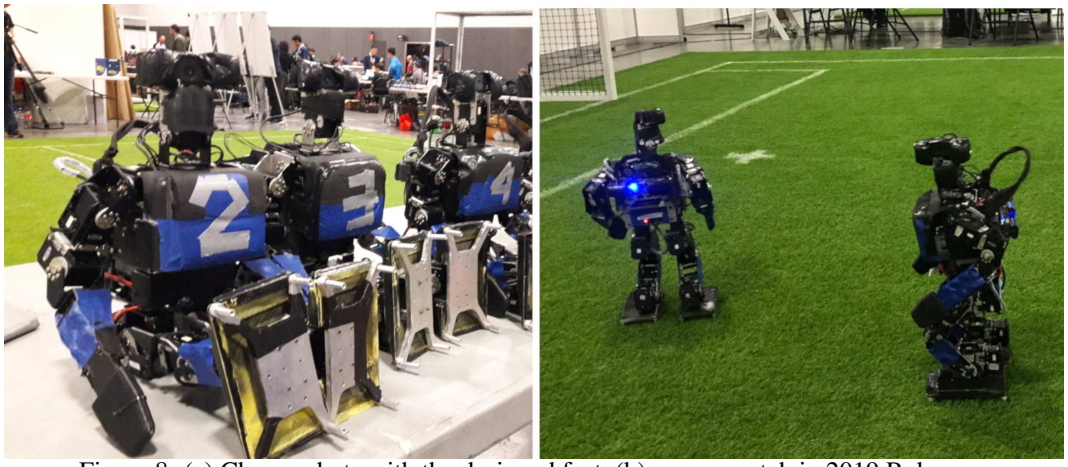

Figure 8: (a) Chape robots with the designed feet, (b) soccer match in 2019 Robocup.

6. REFERENCES

Atmeh, G.M., Ranatunga, I., Popa, D.O., Subbarao, K., Lewis, F. and Rowe, P., 2014. "Implementation of an adaptive, model free, learning controller on the atlas robot". In *2014 American Control Conference*. pp. 2887–2892.

Beer, F.P. and E. R. Johnston, J., 1982. *Resistência dos Materiais*. McGraw-Hill do Brasil.

Comitee, R., 2018. "Robocup soccer humanoid league laws of the game 2017/2018". <https://www.robocuphumanoid.org/materials/rules/>.

Dally, J.W. and Riley, W.F., 1978. *Experimental Stress Analysis*. McGraw-Hill.

Gregoire Passault, e.a., 2015. "Low-cost force sensors for small size humanoid robot". In *15th IEEE-RAS International Conference on Humanoid Robots, Humanoids*. p. 1148.

Ha, I., Tamura, Y. and Asama, H., 2013. "Development of open platform humanoid robot darwin-op". *Advanced Robotics*, Vol. 27, No. 3, pp. 223–232.

Hirai, K., Hirose, M., Haikawa, Y. and Takenaka, T., 1998. "The development of honda humanoid robot". In *Proceedings. 1998 IEEE International Conference on Robotics and Automation*. Vol. 2, pp. 1321–1326.

Radford, N.A.e.a., 2015. "Valkyrie: Nasa's first bipedal humanoid robot". *Journal of Field Robotics*, Vol. 32, No. 3, pp. 397–419.

Raibert, M., Brown Jr., H.B., Chepponis, M., Koechling, J. and Hodgins, J., 1983. "Dynamically Stable Legged Locomotion". Progress Report, Leg Laboratory, Carnegie-Mellon University.

Rotella, N., 2018. *Estimation-Based Control for Humanoid Robots*. Ph.D. thesis, University of Southern California.

S. Kagami, e.a., 2004. "High-speed matrix pressure sensor for humanoid robot by using thin force sensing resistance rubber sheet". In *SENSORS, 2004 IEEE*. Vol. 3, pp. 1534–1537.

Sakagami, Y., Watanabe, R., Aoyama, C., Matsunaga, S., Higaki, N. and Fujimura, K., 2002. "The intelligent asimo: system overview and integration". In *IEEE/RSJ International Conference on Intelligent Robots and Systems*. Vol. 3, pp. 2478–2483.

Schickl, L., Dorer, K., Wülker, M. and Hochberg, U., 2016. "Development of a six-axis force and torque sensor for the humanoid robot sweaty 2.0". In *Proceedings of the 11th Workshop on Humanoid Soccer Robots*.

Vukobratović, M.K. and Okhocimskii, D.E., 1975. "Control of legged locomotion robots". *IFAC Proceedings Volumes*, Vol. 8, No. 1, Part 3, pp. 692 – 704.

7. RESPONSIBILITY NOTICE

The authors are the only responsible for the printed material included in this paper.